1993-07

Multivariable sliding mode control for autonomous diving and steering of unmanned underwater vehicles

Healey, Anthony J.; Lienard, David

IEEE Journal of Oceanic Engineering, Vol. 18, No. 3, July 1993
https://hdl.handle.net/10945/44825

Multivariable Sliding-Mode Control for Autonomous Diving and Steering of Unmanned Underwater Vehicles

Anthony J. Healey and David Lienard

Abstract—**A six degree of freedom model for the maneuvering of an underwater vehicle is used and a sliding mode autopilot is designed for the combined steering, diving, and speed control functions. In flight control applications of this kind, difficulties arise because the system to be controlled is highly nonlinear, coupled, and there is a good deal of parameter uncertainty and variation with operational conditions. The development of variable structure control in the form of sliding modes has been shown to provide robustness that is expected to be quite remarkable for AUV autopilot design. This paper shows that a multivariable sliding mode autopilot based on state feedback, designed assuming decoupled modeling, is quite satisfactory for the combined speed, steering, and diving response of a slow speed AUV. The influence of speed, modeling nonlinearity, uncertainty, and disturbances, can be effectively compensated, even for complex maneuvering. Waypoint acquisition based on line of sight guidance is used to achieve path tracking.**

I. Introduction

THIS PAPER proposes the use of a multivariable sliding mode autopilot for the combined control of AUV steering, depth, and speed during complex flight maneuvers. The method draws upon the power of sliding modes to reduce the inherent coupling between the vehicle response modes that naturally exist in ROV/AUV vehicles. The approach leads to a set of separate designs for the steering, diving, and speed control systems, and a series of simulations based on the dynamics of a swimmer delivery vehicle illustrates the robustness and validity of the concept. This is likely to be the control method of choice for AUV's in the future.

Well-behaved autopilot systems enable the use of a variety of guidance schemes to achieve waypoint and path tracking. Waypoint acquisition is illustrated using proportional line of sight guidance with and without the influence of ocean current. The paper contains a discussion of the vehicle modeling; the sliding mode control design; the guidance scheme; and the results of computer simulations under conditions of parameter mismatch.

II. Background

The design of an autopilot for the control of underwater vehicles is of interest both from the view of motion stabilization as well as maneuvering and tracking performance. AUV's of the class considered here, fall between the two extremes of underwater vehicles (the ROV's and the torpedo type), and are difficult to control having highly variable and uncertain dynamics. Recent work concerned with the modeling and control of ROV vehicles includes Lewis, Lipscomb, and Thompson [14] who described an ROV simulation program using linear hydrodynamic coefficients. ROV vehicles do not possess hydrodynamically shaped profiles and the hydrodynamic forces are uncertain and difficult to predict [4]. To overcome the widely varying and uncertain behavior of these vehicles Russel and Bugge [22] had considered the use of an adaptive automatic guidance system including modeling strong measurement noise of uncertain spectral nature, Yoerger and Slotine [28], [30] proposed and successfully used a sliding mode controller for an ROV maneuvering around large objects at very slow speed; and Goheen, Jefferys, and Broome [12] described a "self testing" procedure for evaluation of the vehicle dynamic response and a corresponding automatic gain selection. In a useful summary of underwater vehicle modeling, Yuh [32] has described the functional form of vehicle dynamic equations of motion, the nature of the loadings and the use of adaptive control via on line parameter identification. The work of Yoerger and Slotine with robust control using sliding modes is most encouraging, and, although the extra time taken to perform the self-test of Goheen *et al.* may not always be available, it still has merit. Recently, Yoerger [30] showed that the dynamics of torque controlled thruster elements are problematic in ROV positioning because lags in the thrust response, if not taken into account, can lead to limit cycling behavior. Fossen [8], and Fossen and Satagun [9] describe the use of multivariable sliding mode control in dynamic positioning of ROV's and show that this method has great potential for controlling the ROV attitude and position with excellent robustness properties against parametric uncertainty.

For higher speed vehicles than ROV's, and those with more streamlined hydrodynamic characteristics, the situation is different, and previous work has been reported by Lindgren *et al.* [17], who addressed the issues of steering and depth control of a torpedo pointing out the importance of the nonlinear hydrodynamic behavior and the stroke limits of the surfaces; Young [31] described the stability derivatives of the Navy's DSRV vehicle, and Smith *et al.* [25] gave a comparison of the performance of a simulator for a swimmer delivery vehicle with field response data. Dobeck *et al.* [6] provided an unclassified description of tests conducted on

Manuscript received November 8, 1991; revised April 23, 1993. This work was supported by the Naval Postgraduate School Direct Research Fund under the technical sponsorship of the Office of Naval Technology.

The authors are with the Department of Mechanical Engineering, Naval Postgraduate School, Monterey, CA 93943.

IEEE Log Number 9211042.

the control systems test vehicle (CSTV) under closed loop computer controlled maneuvering. Humphries [10] describes analytical and empirical considerations for the evaluation of hydrodynamic coefficients while Gueler [11] studied the independent use of bow and stern planes in submarine depth control under the action of wave forces. Richards and Stoten [21], modeling the disturbance response to waves, and later Milliken [18], concerned about the yaw-pitch coupling during turns, applied a linear model based compensator to the problem of depth control. Optimized trade-offs between plane action and the depth error response in waves is possible. So far, the issues of robustness had not been addressed to the same degree as for the ROV vehicles. Milliken described the use of a linearized model-based compensator to reduce the pitch-yaw coupling during turns for a linear submarine vehicle in which a full state observer was employed in the compensator. Some reduction in pitch induced response was achieved depending on speed. A gain schedule with two separate speed regimes was proposed. Consideration was given neither to the design of a command generator nor the feedforward response shaping for depth changing maneuvers. Recently, however, Ruth and Humphreys [23] discussed the use of robust control design using μ synthesis methods in designing the coupled speed/depth controller for a heavy UUV at slow speed where the plane action is used to control both vertical load inbalance and depth. Simulation results indicated that a classical controller could be improved using the 10-state compensator described. Dougherty and Woolweaver [7] have also shown that a mixed sliding mode control with an inner pitch control and outer depth control loop as used on the MUST vehicle provides satisfactory coupled behavior, although the details of the control design are few. Others have suggested the use of sliding modes with adaptivity, as in Cristi *et al.* [3] where the sliding surface is based on system state and state estimators rather than on output error.

It is the robustness of control of UUV's operating in the range up to 10 knots that needs to be addressed, and is the subject of this work. This work shows that a comprehensive multivariable approach to sliding mode autopilot design leads to robustly satisfactory results for flight vehicles, as opposed to ROV's, over a wide speed range. The sliding mode approach used here appears to offer simplicity for vehicle in flight conditions and is similar to that of Fossen and Satagun [9] except in the choice of technique for selection of the sliding surface parameters.

III. Vehicle Modeling

The three-dimensional equations of motion for hydrodynamically shaped underwater vehicles have been described in general terms by Abkowitz [1], and are most conveniently developed using a body fixed coordinate frame and a global reference frame. The body fixed frame has components of motion given by the six velocity components, $[u(t), v(t), w(t), p(t), q(t), r(t)]$, relative to a constant velocity coordinate frame moving with the ocean current, $\boldsymbol{u}_c$, and the velocity vector is represented as

$$\boldsymbol{x}'(t) = [u(t), v(t), w(t), p(t), q(t), r(t)] \tag{1}$$

while the six components of position in the global reference frame are

$$z'(t) = [X(t), Y(t), Z(t), \phi(t), \theta(t), \psi(t)]. \tag{2}$$

The angles $\phi(t)$, $\theta(t)$, $\psi(t)$, (azimuth, elevation, and spin), are related through Euler transformations to the body yaw, pitch, and roll motions. Control inputs from control surfaces, propeller speeds, thruster forces, and buoyancy adjustment in general may be considered as the vector, $\boldsymbol{u}(t)$, and are more specifically taken for this work from a swimmer delivery vehicle, where

$$\boldsymbol{u}'(t) = [\delta_r(t), \delta_{bs}(t), \delta_{bp}(t), \delta_s(t), n(t); B(t)]. \tag{3}$$

The first four correspond to control surface deflections from the rudder, port, and starboard bow planes, and the stern plane, and the remaining two arise from propeller rotational rate and buoyancy adjustment. The development of the functional form of the hydrodynamic forces has been well studied and, in terms of first order variations of motion components, were given by Gertler and Hagen [11] and later by Abkowitz. Specific values of the particular coefficients depend on specific vehicles, although normalization by speed and length can provide some generalized feeling as to their scaling behavior. The values used in this work were based on a box shaped vehicle, a simplified model of which is outlined in the sketch in Fig. 1. This was chosen mainly because experimental data was in existence for the verification of the simulation models used here. The coefficients are vehicle dependent and would need modification if applied to other vehicles. The functional form of the force equations are given in Boncal [2], and are repeated in the Appendix. The model described includes a model of the cross flow drag effects, and a model of the propulsion system and is therefore a large departure from the original work of Abkowitz.

The vehicle motion may be described in terms of the twelve nonlinear system equations [32]

$$\begin{aligned} \boldsymbol{M}(t)d\boldsymbol{x}(t)/dt &= \boldsymbol{f}(\boldsymbol{x}(t), z(t), \boldsymbol{c}(t)) + \boldsymbol{g}(\boldsymbol{x}(t), z(t))\boldsymbol{u}(t) \\ dz(t)/dt &= \boldsymbol{h}(z(t), \boldsymbol{x}(t), \boldsymbol{u}_c) \end{aligned} \tag{4}$$

in which the coupled mass matrix $\boldsymbol{M}(t)$ includes both mechanical and hydrodynamic added mass; the functions $\boldsymbol{f}$ and $\boldsymbol{g}$ are mappings of the vehicle motions into forces including coriolis, gravitational, and centrifugal forces; the hydrostatic and hydrodynamic forces and moments acting on the vehicle in the body fixed coordinate frame, with coefficients $\boldsymbol{c}$; the motion dependent influence of control surfaces, thrusters, and any ballasting; and the function $\boldsymbol{h}$ includes the kinematical relationships found in performing the coordinate transformations between body fixed and global reference frames and the constant ocean current, $\boldsymbol{u}_c$.

Once a hydrodynamic design is made, these functions can be estimated and are known through a vehicle dynamic modeling to lie within a finite bound where that bound can be established *a priori* if knowledge of the variability of the vehicle coefficients $\boldsymbol{c}$ is assumed. The functions $\boldsymbol{f}$ and $\boldsymbol{g}$ are known to be finite gain stable. $\boldsymbol{h}$ is known to be finite gain stable, except at the point where $\theta(t) = \pi/2$. This

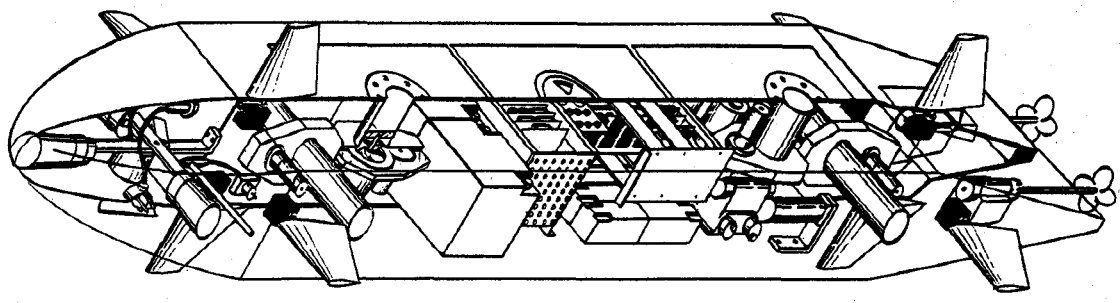

Fig. 1. Sketch of the vehicle type.

singularity may be avoided by the use of quaternions in the rigid body angular motion kinematics rather than Euler angles. In this situation and with (4) as the background model for a general underwater vehicle during maneuvering, the concept of a multivariable sliding mode control will be developed.

IV. Sliding Mode Concepts

We define sliding surfaces in the state error space with the object of finding a sufficient relationship for each of the control element inputs that will guarantee global stability of the state variable errors and provide adequate performance under closed loop conditions. To this end, we define a sliding surface so that each passes through the origin of the state error space. State errors are defined by

$$\begin{bmatrix} \tilde{\boldsymbol{x}}(t) \\ \tilde{\boldsymbol{z}}(t) \end{bmatrix} = \begin{bmatrix} \boldsymbol{x}(t) \\ \boldsymbol{z}(t) \end{bmatrix} - \begin{bmatrix} \boldsymbol{x}(t) \\ \boldsymbol{z}(t) \end{bmatrix}_{\text{com}} \tag{5}$$

where the commands are derived from a consistent command generation system or planned path, or from a series of waypoints corresponding to desired values of vehicle velocity or position (posture). The set of sliding surfaces in the error space are then

$$\boldsymbol{\sigma}(\tilde{\boldsymbol{x}}(t), \tilde{\boldsymbol{z}}(t)) = [\boldsymbol{S}_1 \quad \boldsymbol{S}_2] \begin{bmatrix} \tilde{\boldsymbol{x}}(t) \\ \tilde{\boldsymbol{z}}(t) \end{bmatrix} \tag{6}$$

where

$$\boldsymbol{\sigma}(t) \in \mathcal{R}^{6\times 1};\ \boldsymbol{S}_1, \boldsymbol{S}_2 \in \mathcal{R}^{6\times 6}.$$

Notice that in this work as opposed to the work of Yoerger and Slotine [28], the sliding surfaces are based on state variable errors rather than output errors. For flight vehicles in which the modes are highly coupled, we find this approach to be more flexible. The coefficient matrices $\boldsymbol{S}_1$ and $\boldsymbol{S}_2$ are assumed to be known at this point in the development, although as will be seen, are not arbitrary. In fact, system closed-loop response is dependent on values selected and at least part of any design procedure using sliding mode methods is to properly select surfaces yielding stable closed-loop error dynamics, namely, that for all t and $[\boldsymbol{x}(t), \boldsymbol{z}(t)]$ lying in the space of maneuvers to be accomplished, the conditions

$$\dot{\boldsymbol{\sigma}}(\tilde{\boldsymbol{x}}(t), \tilde{\boldsymbol{z}}(t)) \to 0 \quad \text{as } t \to \infty \tag{7}$$

with

$$\boldsymbol{\sigma}(\tilde{\boldsymbol{x}}(t), \tilde{\boldsymbol{z}}(t)) \to 0 \quad \text{as } t \to \infty \tag{8}$$

will also imply

$$\tilde{\boldsymbol{x}}(t), \tilde{\boldsymbol{z}}(t) \to 0 \quad \text{as } t \to \infty. \tag{9}$$

Global asymptotic stability of the *sliding surface dynamics* is guaranteed through consideration of $\sigma(\tilde{\boldsymbol{x}}(t), \tilde{\boldsymbol{z}}(t))$ in terms of a Lyapunov function $V(\boldsymbol{\sigma}, t)$, yielding

$$V(\boldsymbol{\sigma}(t)) = 0.5\boldsymbol{\sigma}'(\tilde{\boldsymbol{x}}(t), \tilde{\boldsymbol{z}}(t))^*\boldsymbol{\sigma}(\tilde{\boldsymbol{x}}(t), \tilde{\boldsymbol{z}}(t)). \tag{10}$$

Since V is positive definite and radially unbounded, global asymptotic stability of $\boldsymbol{\sigma}(t)$ will be assured if

$$\frac{dV(\boldsymbol{\sigma})}{dt} = \dot{\boldsymbol{\sigma}}\boldsymbol{\sigma} < 0 \qquad \forall t > 0. \tag{11}$$

If we define positive functions $\eta_i(t)$ then global asymptotic stability for the dynamics of each $\sigma_i(t)$ will be given by

$$\dot{\sigma}_i(\tilde{\boldsymbol{x}}(t), \tilde{\boldsymbol{z}}(t)) = -\eta_i \operatorname{sgn}(\sigma(\tilde{\boldsymbol{x}}(t), \tilde{\boldsymbol{z}}(t)) \qquad i = 1, 6. \tag{12}$$

We find it better, in fact, to use a continuous function to define "practical" sliding surface dynamics using a "tanh" function, as in

$$\dot{\sigma}_i(\tilde{x}(t), \tilde{z}(t)) = -\eta_i(t) \tanh(\sigma_i(\tilde{x}(t), \tilde{z}(t))/\phi_i). \tag{13}$$

The powerful result of (13) means that if the η_i are large enough, then in spite of modeling uncertainty, nonlinear terms, and disturbances, the system response will be governed by the response of the $\sigma_i(t)$ and by the choice of the sliding surface parameters: it is less influenced by the parameters of the vehicle dynamics as is more usual with linear feedback controllers. The ϕ_i, not to be confused with the vehicle's roll motion Euler angle $\phi(t)$, are sliding surface boundary layer parameters used to retain continuity of control as motion trajectories cross the sliding surface and prevent chattering. It remains to compute the control law to provide the desired $\boldsymbol{\sigma}$ dynamics and select $\boldsymbol{S}_1$, $\boldsymbol{S}_2$ so that stable dynamics of $\boldsymbol{\sigma}$ results in stability of the tracking errors. Use of the boundary layer to prevent high frequency chattering of the control, however, means that in the presence of uncertainty we can only guarantee global bounded stability for both $\boldsymbol{\sigma}(t)$ and the state errors rather than global asymptotic stability for $\boldsymbol{\sigma}(t)$.

Assuming that $\boldsymbol{S}_{1,2}$ are established (by the method to be described here), substitution of (4) and (6) into (13) yields a solution for the control law.

$$\begin{aligned}\boldsymbol{S}_1\{\boldsymbol{M}^{-1}(t)[\boldsymbol{f}(\boldsymbol{x}(t), \boldsymbol{z}(t), \boldsymbol{c}(t)) + \boldsymbol{g}(\boldsymbol{x}(t), \boldsymbol{z}(t))\boldsymbol{u}(t)] - \dot{\boldsymbol{x}}(t)_{\text{com}}\} \\ + \boldsymbol{S}_2\{\boldsymbol{h}(\boldsymbol{z}(t), \boldsymbol{x}(t), \boldsymbol{u}_c) - \dot{\boldsymbol{z}}(t)_{\text{com}}\} = -\boldsymbol{F}(\boldsymbol{\sigma}, \boldsymbol{\phi}).\end{aligned} \tag{14}$$

Since the $\boldsymbol{f}(\cdot)$, $\boldsymbol{g}(\cdot)$, and $\boldsymbol{h}(\cdot)$ are uncertain in general, we use the estimates, $\hat{\boldsymbol{f}}(\cdot)$, $\hat{\boldsymbol{g}}(\cdot)$, $\hat{\boldsymbol{h}}(\cdot)$, with which the solution for $\boldsymbol{u}(t)$ follows as

$$\boldsymbol{u}(t) = \boldsymbol{u}_1 + \boldsymbol{u}_2 + \boldsymbol{u}_3 \tag{15}$$

where

$$\begin{aligned}
\boldsymbol{u}_1 &= [\hat{\boldsymbol{g}}(\boldsymbol{x}(t), z(t))]^{-1} \\
&\quad \cdot [\{\boldsymbol{S}_1\boldsymbol{M}^{-1}(t)\}^{-1}\dot{\boldsymbol{x}}(t)_{\text{com}} - \hat{\boldsymbol{f}}(\boldsymbol{x}(t), z(t), \boldsymbol{c}(t))] \\
\boldsymbol{u}_2 &= [\hat{\boldsymbol{g}}(\boldsymbol{x}(t), z(t))]^{-1} \\
&\quad \cdot \{\boldsymbol{S}_1\boldsymbol{M}^{-1}(t)\}^{-1}\boldsymbol{S}_2[\dot{z}(t)_{\text{com}} - \hat{\boldsymbol{h}}(z(t), \boldsymbol{x}(t), \boldsymbol{u}_c)] \\
\boldsymbol{u}_3 &= -[\hat{\boldsymbol{g}}(\boldsymbol{x}(t), z(t))]^{-1}\{\boldsymbol{S}_1\boldsymbol{M}^{-1}(t)\}^{-1}\boldsymbol{F}(\boldsymbol{\sigma}, \boldsymbol{\phi})
\end{aligned} \tag{16}$$

and the right-hand side of (13) become the elements of the column vector $\boldsymbol{F}(\boldsymbol{\sigma}, \boldsymbol{\phi})$. The control $\boldsymbol{u}_1$ balances the estimates of the forces to perform the required maneuver, $\boldsymbol{u}_2$ provides stabilization based on estimates of the positional elements in $\boldsymbol{h}$, and the current, and $\boldsymbol{u}_3$ is a switching term that drives the state errors to the sliding surface.

Equation (16) shows a useful structure provided $\boldsymbol{S}_1$ and $\boldsymbol{S}_2$ are known in that $\boldsymbol{u}(t)$ contain feedforward, nonlinear feedback, and nonlinear switching terms that make for inherent robustness. It may be shown that at all times the rank of $[\hat{\boldsymbol{g}}]$ and $[\boldsymbol{S}_1\boldsymbol{M}]$ must be equal to the number of independent control elements; that the system must be controllable; and that the closed-loop behavior on the sliding surface is characterized by 6 poles (same as the number of independent controls) at the origin in the error space; and that $\boldsymbol{S}_1$, $\boldsymbol{S}_2$ may be selected so that stable performance with desired bandwidth is also achieved.

V. Selecting $\boldsymbol{S}_1$, $\boldsymbol{S}_2$ By Linearization and the Equivalent Control

For motions along some nominal flight path, (4) may be linearized into a form in which the linear terms are collected and residuals act as unknown forcing terms. The equations of motion may be linearized for any defined motion using a Taylor series expansion, or by the use of equivalent linearization based on that defined motion, resulting in the following:

$$\begin{aligned}
\begin{bmatrix}\dot{\boldsymbol{x}}(t)\\ \dot{z}(t)\end{bmatrix} &= \begin{bmatrix}\boldsymbol{A}_1 & \boldsymbol{A}_2\\ \boldsymbol{A}_3 & \boldsymbol{A}_4\end{bmatrix}\begin{bmatrix}\boldsymbol{x}(t)\\ z(t)\end{bmatrix} \\
&\quad + \begin{bmatrix}\boldsymbol{B}\\ \boldsymbol{0}\end{bmatrix}\boldsymbol{u}(t) + \boldsymbol{\delta f}(\boldsymbol{x}(t), \boldsymbol{z}(t), \boldsymbol{u}(t), t) \\
&\quad \boldsymbol{A}_1, \boldsymbol{A}_2, \boldsymbol{A}_3, \boldsymbol{A}_4 \in \mathcal{R}^{6\times 6};\ \boldsymbol{B} \in \mathcal{R}^{6\times 6}; \\
&\quad \boldsymbol{u}(t), \boldsymbol{x}(t), \boldsymbol{z}(t) \in \mathcal{R}^{6\times 1}; \\
&\quad \boldsymbol{\delta f}(t) \in \mathcal{R}^{12\times 1}.
\end{aligned} \tag{17}$$

The $\boldsymbol{\delta f}(\cdot)$ contain the differences between linearized and nonlinear accelerations and velocities and are in general uncertain but bounded for bounded motion inputs. In the above it is considered that the mass matrix is nominally constant and invertible and has been multiplied through in the dynamics part of (4). If the nominal path is curved, the dynamics matrix in (17) will be time varying. Assuming that this is not the case, a control based on the linearized motion model would be

$$\begin{aligned}
\boldsymbol{u}(t) &= -[\boldsymbol{S}_1\boldsymbol{B}]^{-1}[\boldsymbol{S}_1 \quad \boldsymbol{S}_2] \\
&\cdot\left\{\begin{bmatrix}\boldsymbol{A}_1 & \boldsymbol{A}_2\\ \boldsymbol{A}_3 & \boldsymbol{A}_4\end{bmatrix}\begin{bmatrix}\boldsymbol{x}(t)\\ z(t)\end{bmatrix} - \begin{bmatrix}\dot{\boldsymbol{x}}(t)\\ \dot{z}(t)\end{bmatrix}^{\text{com}}\right\} - [\boldsymbol{S}_1\boldsymbol{B}]^{-1}\boldsymbol{F}(\boldsymbol{\sigma}, \boldsymbol{\phi}).
\end{aligned} \tag{18}$$

The closed-loop dynamics in a sliding condition are found using the equivalent control defined by Utkin [27]. Also, without loss of generality for the case where the rank of $\boldsymbol{B}$ is full, we can select $\boldsymbol{S}_1$ as unity. Then, if we set $\boldsymbol{F}(\boldsymbol{\sigma}, \boldsymbol{\phi}) = \boldsymbol{0}$ in (18), reduce commands to zero, and realize that not only $\boldsymbol{\sigma}(\boldsymbol{x}(t))$, but also $d\boldsymbol{\sigma}(\boldsymbol{x}(t))/dt$ are zero in the sliding condition, the resulting closed-loop dynamics are given in terms of $\boldsymbol{S}_2$ by

$$\begin{bmatrix}\dot{\boldsymbol{x}}(t)\\ \dot{z}(t)\end{bmatrix} = \begin{bmatrix}-\boldsymbol{S}_2\boldsymbol{A}_3 & -\boldsymbol{S}_2\boldsymbol{A}_4\\ \boldsymbol{A}_3 & \boldsymbol{A}_4\end{bmatrix}\begin{bmatrix}\boldsymbol{x}(t)\\ z(t)\end{bmatrix} \tag{19}$$

and must be designed to be stable.

Since $d\boldsymbol{\sigma}/dt = 0$, $\boldsymbol{\sigma} = 0$, and $\boldsymbol{S}_1 = \boldsymbol{I}$, we can consider $\boldsymbol{x} = -\boldsymbol{S}_2 z$ so that the dynamics of z may be specified to be "desirable" through some closed-loop matrix $\boldsymbol{A}_c$. It may be shown that under these conditions,

$$dz(t)/dt = \boldsymbol{A}_c z(t), \quad \text{where } \boldsymbol{A}_c = (\boldsymbol{A}_4 - \boldsymbol{A}_3\boldsymbol{S}_2). \tag{20}$$

Assuming, as is usually the case, that the pair $(\boldsymbol{A}_4, \boldsymbol{A}_3)$ is controllable, then $\boldsymbol{S}_2$ may be found as a gain matrix for the pair by pole placement or by considering an LQR optimal control solution.

The vehicle dynamics on the sliding surface exhibit equal numbers of integrations as actuation signals hence the benefit in robustness. Having completely designed $\boldsymbol{S}_1$ and $\boldsymbol{S}_2$, (16) provides the control laws. The choice of η_i and ϕ_i are dependent on the activity level desired on the control surfaces and/or thrusters, and on the levels of uncertainty in the estimate of $\boldsymbol{f}(\cdot)$, $\boldsymbol{g}(\cdot)$, $\boldsymbol{h}(\cdot)$.

VI. Solution by Separate Autopilots for Separate Subsystems

The foregoing analysis is, however, not always practical since in flight conditions as opposed to dynamic positioning of ROV's, there are often a smaller number of independent actuators than degrees of freedom. For instance, both pitch and heave modes are controlled by dive planes. The choice of $\boldsymbol{S}_1 = \boldsymbol{I}$ is therefore not always valid and $\boldsymbol{B}$ is possibly rank deficient in these cases. We seek an alternative solution approach by separating the system into noninteracting (or lightly interacting) subsystems, grouping certain key motion equations together for the separate functions of steering, diving, and speed control. Other modes of response such as roll are commonly left as passive—as is the case here. For dynamic positioning control we would return to the case of full rank for $\boldsymbol{B}$ and proceed as earlier outlined.

Restructuring (17) we get for each of four subsystems

$$\begin{aligned}
d\boldsymbol{x}_i(t)/dt &= \boldsymbol{A}_i\boldsymbol{x}_i(t) + \boldsymbol{b}_i u_i(t) \\
&\quad + \boldsymbol{\delta f}_i(\boldsymbol{x}_i(t), \boldsymbol{x}_j(t), u_j(t), t) \\
&\quad i = 1, \ldots, 4 \quad j = 1, \ldots, 4
\end{aligned} \tag{21}$$

TABLE I
TABLE OF SUBSYSTEM STATES AND INPUTS

Speed Control States:	
$\boldsymbol{x}_1'(t) = [u(t)];$	$u_1(t) = n(t)$
Steering System States:	
$\boldsymbol{x}_2'(t) = [v(t), r(t), \psi(t)];$	$u_2(t) = \delta_r(t)$
Diving System States:	
$\boldsymbol{x}_3'(t) =$	$u_3(t) = \delta_s(t)$
$[w(t), q(t), \theta(t), Z(t)];$	

and the $\boldsymbol{\delta f}_i$ represent nonlinear and coupling terms as functions of the coupling motions $\boldsymbol{x}_j(t)$ and other controls $\boldsymbol{u}_j(t)$. In particular, the four subsystems correspond to the speed, steering, diving, and roll control modes. The fourth system (roll) remains passively stable without active control ($u_4(t) = 0$).

VII. Control Philosophy for the Three Autopilots

A philosophy of control which is derived by the particular choice of subsystem equations is that the steering system will be responsible for control of the heading errors; the diving system will be responsible for the depth and pitch errors; and the speed system will control to speed commands. It should be pointed out that this control philosophy maps directly with the current practice in naval submarines. The conversion of commands for path following to a global location (X, Y, Z) will be accomplished by a guidance law that is the interesting subject of work addressed in later sections of the paper, and by others such as Papoulias [19].

With only a single control element active each subsystem, may be treated separately as a single input, multistate (SIMS) system with its own single sliding surface definition. We proceed to define

$$\sigma_1(t) = \boldsymbol{s}_1.\tilde{\boldsymbol{x}}_1(t); \quad \sigma_2(t) = \boldsymbol{s}_2.\tilde{\boldsymbol{x}}_2(t); \quad \sigma_3(t) = \boldsymbol{s}_3.\tilde{\boldsymbol{x}}_3(t). \tag{22}$$

VIII. SIMS Design Method

For any subsystem where

$$\dot{\boldsymbol{x}}(t) = \boldsymbol{A}\boldsymbol{x}(t) + \boldsymbol{b}\boldsymbol{u}(t) + \boldsymbol{\delta f}(t) \tag{23}$$

and

$$\boldsymbol{x}(t) \in \mathcal{R}^{n\times 1}; \ \boldsymbol{b} \in \mathcal{R}^{n\times 1}; \ \boldsymbol{A} \in \mathcal{R}^{n\times n}.$$

If the pair ($\boldsymbol{A}$, $\boldsymbol{b}$) is controllable, and [$\boldsymbol{s}'\boldsymbol{b}$] is nonzero, then it may be shown (see [5] and [27] for a comprehensive tutorial) that the sliding surface coefficients are elements of the left eigenvector of the closed-loop dynamics matrix $\boldsymbol{A}_c$ corresponding to a pole at the origin

$$\boldsymbol{s}'[\boldsymbol{A}_c] = 0 \tag{24}$$

and the matrix $\boldsymbol{A}_c$ is given by

$$\boldsymbol{A}_c = [\boldsymbol{A} - \boldsymbol{b}\boldsymbol{k}']$$

where $\boldsymbol{k}$ is the gain vector that places the closed-loop poles of the system at

$\lambda_1 = 0$, and λ_i, $i = 2$, n are selected for performance.

The resulting sliding control law including the estimate $\boldsymbol{\delta}\hat{\boldsymbol{f}}(t)$ of the uncertain disturbance $\boldsymbol{\delta f}(t)$ becomes

$$u(t) = [\boldsymbol{s}'\boldsymbol{b}]^{-1}[-\boldsymbol{s}'\boldsymbol{A}\boldsymbol{x}(t) - \boldsymbol{s}'\boldsymbol{\delta}\hat{\boldsymbol{f}}(t) + \boldsymbol{s}'\dot{\boldsymbol{x}}_{\text{com}}(t) - \eta \tanh(\sigma(t)/\phi)] \tag{25}$$

or

$$u(t) = -\boldsymbol{k}'\boldsymbol{x}(t) - [\boldsymbol{s}'\boldsymbol{b}]^{-1}\boldsymbol{s}'\boldsymbol{\delta}\hat{\boldsymbol{f}}(t) + [\boldsymbol{s}'\boldsymbol{b}]^{-1}\boldsymbol{s}'\dot{\boldsymbol{x}}_{\text{com}}(t) - [\boldsymbol{s}'\boldsymbol{b}]^{-1}\eta\tanh(\sigma(t)/\phi). \tag{26}$$

The choice of the switching gain, $\eta(t)$ and the "boundary layer thickness" ϕ, is selected to eliminate control chattering. Reducing ϕ increases the nonlinear gain at small σ, while increasing ϕ introduces a filtering effect if measurements are noisy. Further details are given in Sur [26] and Lienard [16].

The excellent robustness attributed to the sliding control method can be clarified by recasting the closed-loop equations of motion using (26) to get

$$\dot{\boldsymbol{x}}(t) = [\boldsymbol{A} - \boldsymbol{b}\boldsymbol{k}]\boldsymbol{x}(t) + \dot{\boldsymbol{x}}_{\text{com}}(t) - \boldsymbol{\delta}\hat{\boldsymbol{f}}(t) + \boldsymbol{\delta f}(t) - \boldsymbol{b}[\boldsymbol{s}'\boldsymbol{b}]^{-1}\eta \tanh(\sigma(t)/\phi) \tag{27}$$

and since

$$\dot{\sigma}(t) = \boldsymbol{s}'(\boldsymbol{x}(t) - \boldsymbol{x}_{\text{com}}(t)) \tag{28}$$

we get

$$\dot{\sigma}(t) = -\eta \tanh(\sigma(t)/\phi) + \boldsymbol{s}'[\boldsymbol{\delta f}(t) - \boldsymbol{\delta f}!a5(t)]. \tag{29}$$

Thus so long as η is chosen to be "large enough" to overcome the destabilizing effects of any disturbance mismatch, *bounded stability* of the errors is assured even though asymptotic stability is only approached as ϕ tends to zero. In this case η is selected so that

$$\eta > \|\boldsymbol{s}\| \ \|[\boldsymbol{\delta f}(t) - \boldsymbol{\delta}\hat{\boldsymbol{f}}(t)]\| \tag{30}$$

and ϕ is selected between 0.05 and 0.2.

IX. Speed Control Autopilot

The longitudinal equation of motion, neglecting the effects of plane drag, is

$$\dot{u}(t) = -\alpha u(t)|u(t)| + (\alpha\beta)n(t)|n(t)| \tag{31}$$

where

$$\alpha = \frac{\rho L^2 C_d}{[2m + \rho L^3 X_{\dot{u}}]}, \quad \beta = u_0^2/n_0^2 \quad \text{and} \quad C_d = 0.0034$$

and is linear in the modified square of the vehicle and propulsor speeds. The sliding surface for the speed control autopilot is thus first order and, without loss of generality, we can select $\sigma_1 = 1$ so that

$$\sigma_1(t) = u(t) - u_{\text{com}}(t) = \tilde{u}(t) \tag{32}$$

with the result that the control law in terms of the command for $n(t)$ is found from

$$\dot{\sigma}_1(t) = -\eta_1\tanh(\sigma_1(t)/\phi_1) \tag{33}$$

TABLE II

$Y_1 = 0.5\rho L^2 Y_v$	$N_1 = 0.5\rho L^3 N_v$
$Y_2 = 0.5\rho L^3 Y_r$	$N_2 = 0.5\rho L^4 N_r$
$Y_3 = 0.5\rho L^2 u^2 Y_{\delta r}$	$N_3 = 0.5\rho L^3 u^2 N_{\delta r}$

giving

$$n(t)|n(t)| = (\alpha\beta)^{-1}\{\alpha u(t)|u(t)| + \dot{u}_{\rm com}(t) - \eta_1 \tanh(\sigma_1(t)/\phi_1)\} \quad (34)$$

so that $n(t)$ = signed square root of the right-hand side of (34). Notice that the propeller speed command arises from one term to accelerate the vehicle, another to overcome the vehicle forward drag, and the last term to stabilize the motion.

X. Steering Autopilot

The linearized steering system dynamics are given by the third-order system

$$\begin{aligned} m_1\dot{v}(t) + m_2\dot{r}(t) &= Y_1 uv(t) + Y_2 ur(t) + Y_2\delta_r(t) \\ m_3\dot{v}(t) + m_4\dot{r}(t) &= N_1 uv(t) + N_2 ur(t) + N_3\delta_r(t) \\ \dot{\psi}(t) &= r(t) \end{aligned} \quad (35)$$

while the progression of vehicle position not included in the autopilot system dynamics is given by

$$\begin{aligned} \dot{X}(t) &= u(t)\cos\psi(t) - v(t)\sin\psi(t) + u_{cx} \\ \dot{Y}(t) &= u(t)\sin\psi(t) + v(t)\cos\psi(t) + u_{cy} \end{aligned} \quad (36)$$

where the coefficients Y and N are given in Table II in terms of the nondimensional hydrodynamic coefficients of the Appendix.

By inversion of the mass matrix, (19) may be expressed as

$$\dot{\boldsymbol{x}}_2(t) = \boldsymbol{A}_2\boldsymbol{x}_2(t) + \boldsymbol{b}_2 u_2(t) \quad (37)$$

where

$$\boldsymbol{A}_2 \begin{bmatrix} \begin{bmatrix} m_1 & m_2 \\ m_3 & m_4 \end{bmatrix}^{-1} & \begin{bmatrix} Y_1 & Y_2 \\ N_1 & N_2 \end{bmatrix} & \begin{matrix} 0 \\ 0 \end{matrix} \\ \begin{matrix} 0 & 0 \end{matrix} & & 1 \end{bmatrix}$$

$$\boldsymbol{b}_2 = \begin{bmatrix} \begin{bmatrix} m_1 & m_2 \\ m_3 & m_4 \end{bmatrix}^{-1} & \begin{bmatrix} Y_3 \\ N_3 \end{bmatrix} \\ \begin{matrix} 0 & 0 \end{matrix} & \end{bmatrix} \quad (38)$$

or, in more detail as

$$\begin{bmatrix} \dot{v}(t) \\ \dot{r}(t) \\ \dot{\psi}(t) \end{bmatrix} = \boldsymbol{A}_2 \begin{bmatrix} v(t) \\ r(t) \\ \psi(t) \end{bmatrix} + \boldsymbol{b}_2\delta_r(t)$$

$$\boldsymbol{A}_2 \in \mathcal{R}^{3\times 3}; \quad \boldsymbol{b}_2 \in \mathcal{R}^{3\times 1}. \quad (39)$$

Defining the sliding surface for steering as $\sigma_2(t)$, the values to place the sliding poles of the steering system arbitrarily at $[0 \quad -0.41 \quad -0.42]$ become

$$\sigma_2(t) = -0.074\tilde{v}(t) + 0.816\tilde{r}(t) + 0.573\tilde{\psi}(t) \quad (40)$$

and the steering control law results in

$$\delta_r(t) = 0.033v(t) + 0.1112r(t) + 2.58\tanh\{[0.074\tilde{v}(t) + 0.816\tilde{r}(t) + 0.573\tilde{\psi}(t)]/0.1\}. \quad (41)$$

Notice that in the above, the heading error term is only included in the nonlinear switching term, while the linear feedback of $v(t)$ and $r(t)$ act only to stabilize the sway/yaw dynamics. The heading rate, $r_{\rm com}(t)$ is set to zero here although in rate command maneuvers it should also be included in the switching term as well as in the rate command term in the control law. $v_{\rm com}(t)$ is not practical to include. Further details of the speed and steering autopilots are given in [16].

XI. Diving Autopilot

The linearized diving system dynamics are given by the system of equations

$$\begin{bmatrix} \dot{q}(t) \\ \dot{\theta}(t) \\ \dot{Z}(t) \end{bmatrix} = \begin{bmatrix} -0.7 & -0.3 & 0 \\ 1 & 0 & 0 \\ 0 & -u_0 & 0 \end{bmatrix} \begin{bmatrix} q(t) \\ \theta(t) \\ Z(t) \end{bmatrix} + \begin{bmatrix} 0.035 \\ 0 \\ 0 \end{bmatrix} \delta_s(t). \quad (42)$$

In the above, the influence of $w(t)$, which may be significant in some vehicles, is in fact small in this case, perhaps because of the rectangular cross section. The sliding surface for the diving autopilot ignoring any nonzero command for pitch for now then becomes

$$\sigma_3(t) = \tilde{q}(t) + 0.520\tilde{\theta}(t) - 0.011\tilde{Z}(t) \quad (43)$$

when the poles are placed at $[0 \quad -0.25 \quad -0.26]$. With $[\boldsymbol{s}'\boldsymbol{b}]^{-1}\eta = 4.0$ and $\phi = 0.4$ the autopilot will have relatively fast performance. Externally to the computation of $\delta_s(t)$, it is necessary to limit commands for control surface stroke to a value, in this case, of 0.4 radians. The final diving control law is [26]

$$\delta_s(t) = -5.143q(t) + 1.070\theta(t) + 4.000\tanh[\sigma_3(t)/0.4]. \quad (44)$$

XII. Composite Control Results by Simulation

Two types of simulation can lead to an understanding of the performance of the three autopilot systems; by simulation of the linearized closed-loop performance; and, by simulation of the complete nonlinear coupled system under the action of the autopilots designed by the separate linearized procedure. We will show first that each individual system response is well behaved when controlling a linearized uncoupled vehicle model. Secondly, we will show that the combined autopilot system is effective in driving the full nonlinear vehicle model through both steering and diving maneuvers as well as acceleration to speed. These complex maneuvers are significant because the additional drag terms due to control surface action cause a significant departure of the dynamics from the linear case. Also, the changing speed influences the unmodeled nonlinearity.

In Figs. 2 and 3, simulations are based on a time step of 0.1 s for 750 time steps and show the performance of separate speed control and heading autopilots in commands from 0 to 90° and 0 to a commanded cruise speed of two-thirds of the nominal speed of 1.832 m/s. The results are normalized because normalized equations of motion in ship maneuvering work show that under some conditions speed effects may be reducible to a second order effect. Distance is conveniently

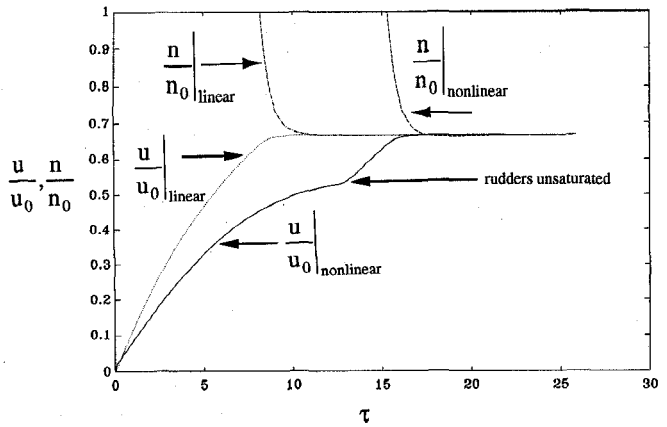

Fig. 2. Vehicle closed-loop speed and propeller response in accelerating zero to commanded speed: Linear and nonlinear compared: $u_{\text{com}} = 0.67u_0$.

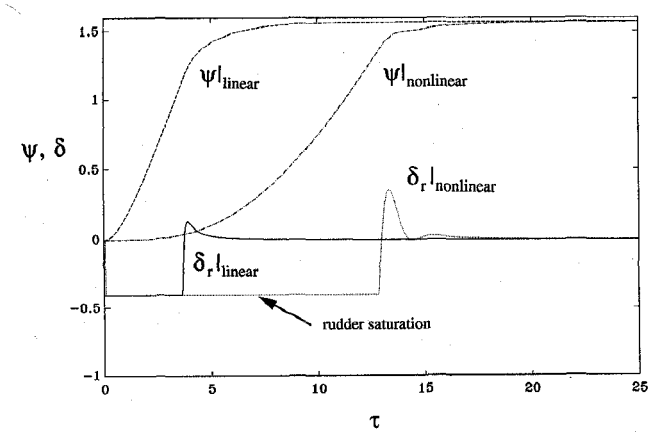

Fig. 3. Vehicle rudder and yaw response in accelerating from zero to commanded speed and turning 90°: Liner and nonlinear compared.

normalized by the ship length, L. Normalized time, τ, is conveniently expressed in time to transit one ship length at the forward speed u ($\tau = tu/L$). Also, as a wide speed range is contemplated, normalized data can be shown on fewer plots. Naturally, results computed for the same total real time at different speeds will have different nondimensional time spans which is why some later plots end at different points.

Figure 2 shows a comparison of linear and nonlinear normalized propulsion motor speed and vehicle speed on the same plot versus normalized time. The normalizing parameters correspond to a propeller speed of 52.359 rad/s which drives the vehicle to a nominal speed of u_0 of 1.832 m/s. The steering responses shown in Fig. 3 compare the linear and nonlinear systems behavior through the 90° turn. The rudder commands are saturated at 0.4 rad. The proof of concept is given in Figs. 2 and 3 in which the autopilots appear to control the full nonlinear vehicle model in adequate fashion during a combined maneuver, accelerating to speed with a hard turn to port, in spite of the variation between the linear and nonlinear vehicle dynamics.

While the closed loop performance of the nonlinear model takes longer to accelerate to speed, it is clear from Fig. 3 that, even though additional overshoot in rudder action is required in coming out of the turn, stable response is still achieved. The nonlinear vehicle speed response also clearly shows the added acceleration at $\tau = 12.5$ associated with drag loss when the rudder action is reduced.

XIII. Combined Maneuvering at Higher Speed

It is interesting to determine if an autopilot designed for slow speed will also control the vehicle in higher speed maneuvers. Without modification to the control laws, the series of Fig. 4 show that a complex maneuver, diving to a depth increase of 2 vehicle lengths, turning 90° to port, and maintaining speed in the turn, is controlled with changes in response but without loss of stability. Each figure in the series shows results for 1.0, 1.2, 2.0, and 3.0 times the nominal speed. The simulations were run with initial conditions corresponding to a nominal straight line flight along the global X axis at the appropriate speed with the maneuver initiated at $t = 0.0$. Figs. 4(a) and (b) show the steering response with ψ in degrees and δ_r in radians. The time for each case is nondimensionalized using the appropriate speed so each case in Fig. 4 terminates at different values of τ. In Fig. 4(b), the initial maneuver causes the control surface to saturate at 0.4 rad for some time before the controller acts to stabilize the turn. Since the maneuvers occur at different speeds, the time to make the turn and the response of the rudder command is different for each case. Figs. 4(c) and (d) show the diving response; Figs. 4(e) and (f) show the propeller and vehicle speed responses where the initial conditions are normalized to 1.0; Figs. 4(g) and (h) show the pitch and roll responses in degrees respectively; and, Fig. 4(i) shows the differences in the vehicle's path for each case. In spite of what is shown in Fig. 1, the vehicle model includes a keel which has the effect of inducing a sway coupled roll motion. The combined maneuver causes the vehicle to roll up to 35° during the turn which modifies the effectiveness of the control planes in their respective steering and diving functions. In developing these results a time step of 0.018 s for 1000 time steps was used to maintain numerical stability with the Euler integration scheme. The responses are plotted against nondimensionalized time (distance traveled in ship lengths) to enhance the comparison of the effect of speed. The vehicle physical response time increases with speed as the restoration forces from gravity and buoyancy become weaker compared to the hydrodynamic body forces, and responses at increasing speed are characterized by increased damping. At slow speed the vehicle input response (Fig. 4(b)) shows that more rudder overshoot is needed to stabilize the vehicle as it exits the turn, but the robustness of the sliding mode controller is such that stability is still retained.

XIV. Waypoint Guidance by Line of Sight

Vehicle autonomous guidance is most simply accomplished by a heading command to the vehicle's steering system to approach the line of sight between the present position of the vehicle and the waypoint to be reached. In missile guidance this is related to "proportional navigation." The difference in guiding AUV's is that the vehicle response is slow compared to the rates of change in command unless the waypoint is many

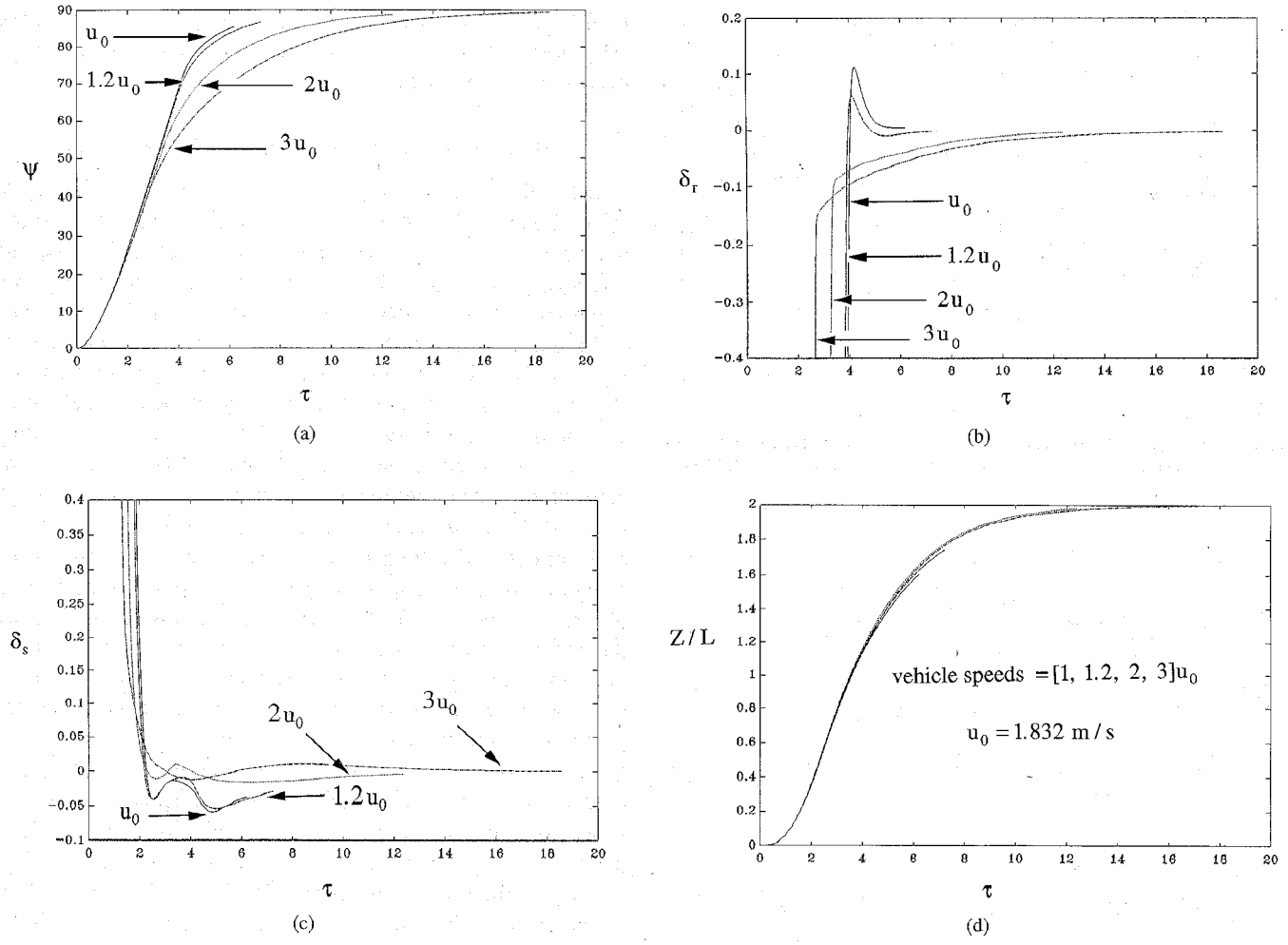

Fig. 4. (a) Combined maneuver responses: All three autopilots acting together, robustness to speed: steering response—yaw (y degrees) versus time (τ). (b) Steering responses—rudder command (δ_s) versus time (τ). (c) Diving responses—stern plane command (δ_s) versus time (τ). (d) Diving responses—depth (Z/L) versus time (τ) *(Continued)*.

vehicle lengths away. Separation of guidance and autopilot functions may not always produce stable results underwater. Notwithstanding, we define the line of sight (LOS) to be the horizontal plane angle given by

$$\psi_{\text{com}} = \tan^{-1}\left[\frac{(Y_k - Y(t))}{(X_k - X(t))}\right] \tag{45}$$

in which the $[X_k, Y_k]$ are waypoints stored in the vehicle's mission planner. Care must be taken to keep the proper quadrant in mind when programming the guidance law. The decision as to whether the waypoint has been reached is made on the basis of whether the vehicle lies within a "ball of acceptability," ρ_0 defined around the particular waypoint. Namely, if, for some distance, ρ_0, an acceptable zone around the waypoint, $[X_k(t), Y_k(t), Z_k(t)]$, the vehicle location $[X(t), Y(t), Z(t)]$ are such that

$$\rho^2(t) = [Y_k - Y(t)]^2 + [X_k - X(t)]^2 + \lambda[Z_k - Z(t)]^2 < \rho_0^2 \qquad 0 < \lambda < 1 \tag{46}$$

then (46) triggers the selection of the next waypoint. If, on the other hand, the condition that $d\rho/dt$ goes from negative to positive without the above being met then the waypoint is not reached. At this juncture, the guidance law must contain logic that will either hold the current waypoint, directing the vehicle to circle, or enter the next, depending on a mission planning decision. λ is a parameter relating to the importance of including the depth dimension. In this section, vehicle waypoint control is examined in simulations using the autopilots described above combined with the LOS guidance. The assumption is made that vehicle speed control is obtained from a separate speed command for each separate leg of a transit mission, although that could be accomplished also by an on line speed command as a function of distance to go and the time to go if a desired time is also associated with each waypoint. The performance of the LOS method is illustrated in Fig. 5 showing that the large overshoot is natural when path dimensions are not large compared to the vehicle turning radius, and when the commanded heading change is large. These simulations are for a "ball of acceptability" of radius equal to two ship lengths run at the nominal vehicle speed. The results show that precision path following in tight maneuvering is not readily obtained using LOS and that more sophisticated guidance schemes including vehicle lags in the path planning are needed. One

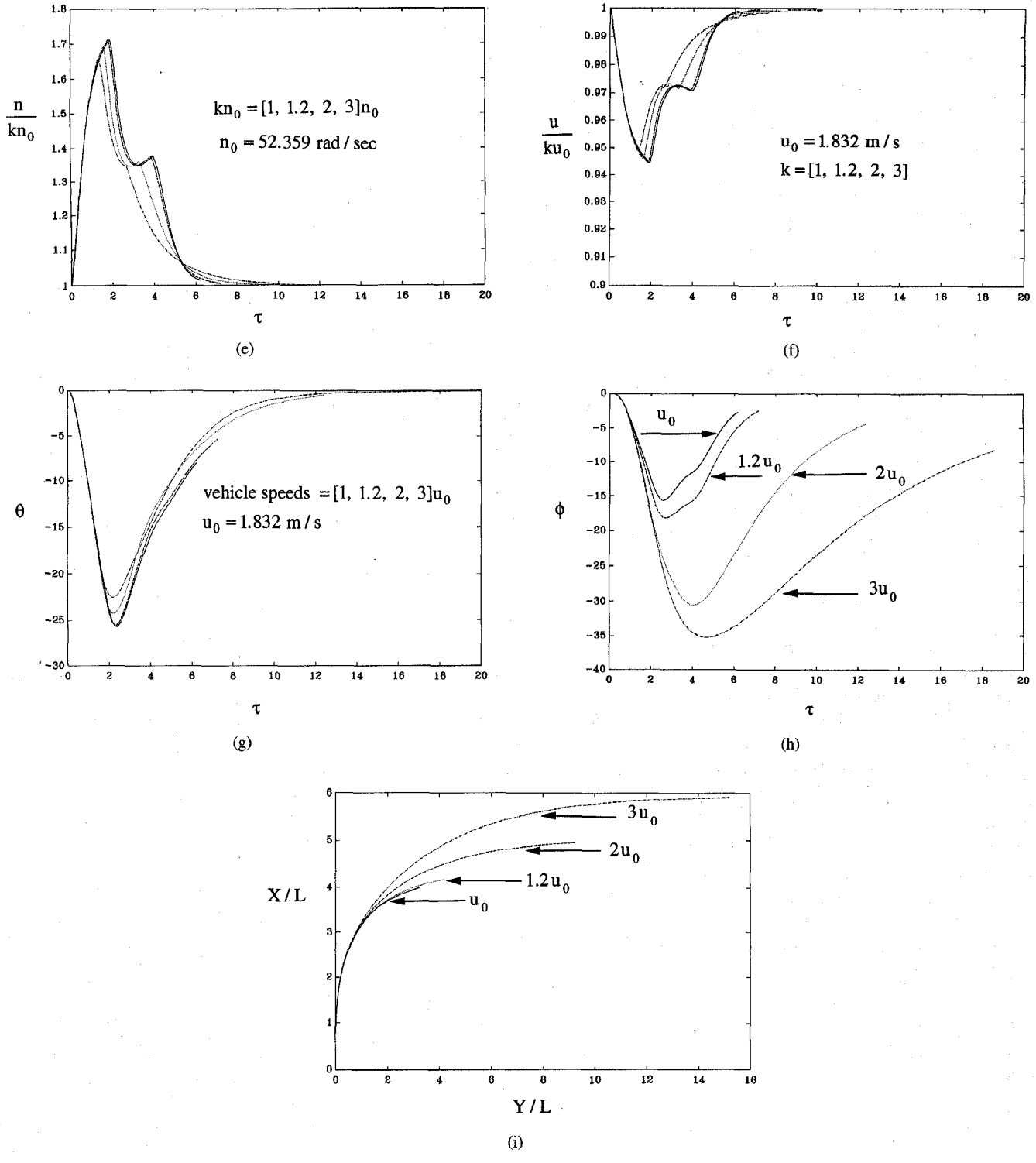

Fig. 4. *(Continued)* (e) Propeller rate responses—normalized propeller rate versus time (τ). (f) Vehicle speed responses—normalized forward velocity versus time (τ). (g) Vehicle pitch angle responses—pitch (θ) versus time (τ). (h) Vehicle roll angle responses—roll (ϕ) versus time (τ). (i) Vehicle path responses, distance in ship lengths—X/L versus Y/L.

possible scheme involves cross track error minimization and is attractive but more involved than LOS in its implementation.

XV. Effect of Ocean Current

Finally, the influence of ocean current in slow speed guidance is that waypoints may not be achievable under the most unfavorable circumstances and that the vehicle track tends to fall downstream of the desired track. Figure 5 illustrates that without current compensation, slow-speed AUV's may have difficulty in precision control. The case of a current at 45° to the $[X, Y]$ axis of magnitude 0.23 times the vehicle nominal speed shows the magnitude of the track errors obtained. It

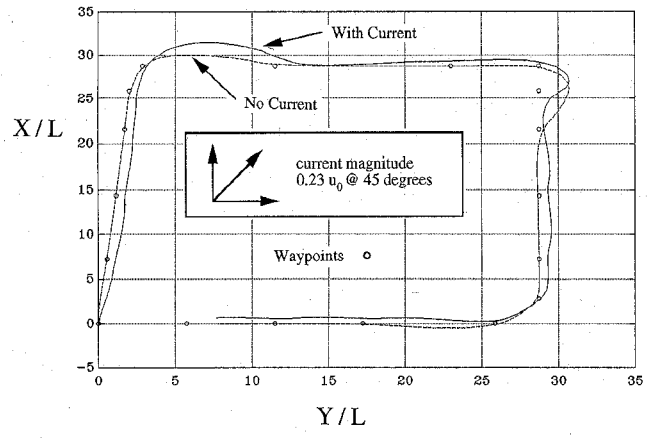

Fig. 5. Waypoint following, LOS guidance: $\rho_0 = 2L$ at nominal speed u_0, with and without current, with specified waypoints shown.

should be noted that the ratio of the current to vehicle speed is much higher in AUV's than in higher speed vehicles. With current included as an added state in the sliding surface definition, and assumed to be measurable, the original track without current can be recovered. There is a steady offset in the vehicle heading to compensate for the current effect.

XVI. Conclusions

In conclusion, the use of sliding mode methods has been shown to provide robust performance of underwater vehicle autopilots when designed separately for speed control, steering, and diving activity. The method is generally suitable for a wide variety of nonlinear control problems although for flight conditions, may be implemented using a linearized model for the sliding surface coefficient design. A study of waypoint acquisition using a LOS guidance has shown that the scheme is robust but not accurate in tight turning maneuvers. Path planning algorithms must take vehicle dynamics into account. Ocean currents effect the ability of the LOS guidance to drive the vehicle to its desired waypoint and must be compensated by an added feedforward term in the steering controller based on a current magnitude and direction estimate.

Acknowledgment

The authors wish to thank the reviewers for helpful comments.

Appendix
(Nomenclature according to Lewis [15])

XIX. Surge Motion Equation

$$m[\dot{u} - vr + wq - x_G(q^2 + r^2) + y_G(pq - \dot{r}) + Z_G(pr + \dot{q})] = \frac{\rho}{2}L^4[X_{pp}p^2 + X_{qq}q^2 + X_{rr}r^2 + X_{pr}pr] + \frac{\rho}{2}L^3[X_{\dot{u}}\dot{u} + X_{wq}wq + X_{vp}vp + X_{vr}vr + uq(X_{q\delta s}\delta_s + X_{q\delta b/2}\delta_{bp} + X_{q\delta b/2}\delta_{bs}) + X_{r\delta r}ur\delta_r] + \frac{\rho}{2}L^2[X_{vv}v^2 + X_{ww}w^2 + X_{v\delta r}uv\delta_r + uw(X_{w\delta s}\delta_s + X_{w\delta b/2}\delta_{bs} + X_{w\delta b/2}\delta_{bp}) + u^2(X_{\delta s\delta s}\delta_s^2 + X_{\delta b\delta b/2}\delta_{\delta b}^2 + X_{\delta r\delta r}\delta_r^2)] - (W - B)\sin\theta + \frac{\rho}{2}L^3X_{q\delta sn}uq\delta_s\epsilon(n) + \frac{\rho}{2}L^2[X_{w\delta sn}uw\delta_{sn} + X_{\delta s\delta sn}u^2\delta_s^2] \cdot \epsilon(n) + \frac{\rho}{2}L^2u^2X_{\text{prop}}.$$

Sway Motion Equation

$$m[\dot{v} + ur - wp + x_G(pq + \dot{r}) - y_G(p^2 + r^2) + z_G(qr - \dot{p})] = \frac{\rho}{2}L^4[Y_{\dot{p}}\dot{p} + Y_{\dot{r}}\dot{r} + Y_{pq}pq + Y_{qr}qr] + \frac{\rho}{2}L^3[Y_{\dot{v}}\dot{v} + Y_pup + Y_rur + Y_{vq}vq + Y_{wp}wp + Y_{wr}wr] + \frac{\rho}{2}L^2[Y_vuv + Y_{vw}vw + Y_{\delta r}u^2\delta r] - \frac{\rho}{2}\int_{x_{\text{tail}}}^{x_{\text{nose}}}[C_{dy}h(x)(v + xr)^2 + C_{dz}b(x)(w - xq)^2] \cdot \frac{(v + xr)}{U_{cf}(x)}dx + (W - B)\cos\theta\sin\phi.$$

Heave Motion Equation

$$m[\dot{w} - uq + vp + x_G(pr - \dot{q}) + y_G(qr + \dot{p}) - z_G(p^2 + q^2)] = \frac{\rho}{2}L^4[Z_{\dot{q}}\dot{q} + Z_{pp}p^2 + Z_{pr}pr + Z_{rr}r^2] + \frac{\rho}{2}L^3[Z_{\dot{w}}\dot{w} + Z_quq + Z_{vp}vp + Z_{vr}vr] + \frac{\rho}{2}L^2[Z_wuw + Z_{vv}v^2 + u^2(Z_{\delta s}\delta_s + Z_{\delta b/2}\delta_{bs} + Z_{\delta b/2}\delta_{bp})] + \frac{\rho}{2}\int_{x_{\text{tail}}}^{x_{\text{nose}}}[C_{dy}h(x)(v + xr)^2 + C_{dz}b(x)(w - xq)^2]\frac{(w - xq)}{U_{cf}(x)}dx + (W - B)\cos\theta\cos\phi + \frac{\rho}{2}L^3Z_{qn}uq\epsilon(n) + \frac{\rho}{2}L^2[Z_{wn}uw + Z_{\delta sn}u^2\delta_s]\epsilon(n).$$

Roll Motion Equation

$$I_x\dot{p} + (I_z - I_y)qr + I_{xy}(pr - \dot{q}) - I_{yz}(q^2 - r^2) - I_{xz}(pq + \dot{r}) + m[y_G(\dot{w} - uq + vp) - z_G(\dot{v} + ur - wp)] + \frac{\rho}{2}L^5[K_{\dot{p}}\dot{p} + K_{\dot{r}}\dot{r} + K_{pq}pq + K_{qr}qr] + \frac{\rho}{2}L^4[K_{\dot{v}}\dot{v} + K_pup + K_rur + K_{vq}vq + K_{wp}wp + K_{wr}wr] + \frac{\rho}{2}L^3[K_vuv + K_{vw}vw + u^2(K_{\delta b/2}\delta_{bp} + K_{\delta b/2}\delta_{bs})] + (y_GW - y_BB)\cos\theta\cos\phi - (z_GW - z_GB)\cos\theta\sin\phi + \frac{\rho}{2}L^4K_{pn}up\epsilon(n) + \frac{\rho}{2}L^3u^2K_{\text{prop}}.$$

Pitch Motion Equation

$$
\begin{aligned}
&I_y\dot{q} + (I_x - I_z)pr - I_{xy}(qr + \dot{p}) + I_{yz}(pq - \dot{r}) \\
&\quad + I_{xz}(p^2 - r^2) - m[x_G(\dot{w} - uq + vp) - z_G(\dot{u} - vr + wq)] \\
&\quad = \frac{\rho}{2}L^5[M_{\dot{q}}\dot{q} + M_{pp}p^2 + M_{pr}pr + M_{rr}r^2] \\
&\quad + \frac{\rho}{2}L^4[M_{\dot{w}}\dot{w} + M_{uq}uq + M_{vp}vp + M_{vr}vr] \\
&\quad + \frac{\rho}{2}L^3[M_{uw}uw + M_{vv}v^2 + u^2(M_{\delta s}\delta_s \\
&\quad + M_{\delta b/2}\delta_{bp} + M_{j\delta b/2}\delta_{bs})] \\
&\quad - \frac{\rho}{2}\int_{x_{\text{tail}}}^{x_{\text{nose}}}[C_{dy}h(x)(v + xr)^2 + C_{dz}b(x)(w - xq)^2] \\
&\quad \cdot \frac{(w + xq)}{U_{cf}(x)}xdx - (x_GW - x_BB)\cos\theta\cos\phi \\
&\quad - (z_GW - z_BB)\sin\theta + \frac{\rho}{2}L^4M_{qn}uq\epsilon(n) \\
&\quad + \frac{\rho}{2}L^3[M_{wn}uw + M_{\delta sn}u^2\delta_s]\epsilon(n).
\end{aligned}
$$

Yaw Motion Equation

$$
\begin{aligned}
&I_z\dot{r} + (I_y - I_x)pq - I_{xy}(p^2 - q^2) - I_{yz}(pr + \dot{q}) \\
&\quad + I_{xz}(qr - \dot{p}) + m[x_G(\dot{v} + ur - wp) \\
&\quad - y_G(\dot{u} - vr + wq)] \\
&\quad = \frac{\rho}{2}L^5[N_{\dot{p}}\dot{p} + N_{\dot{r}}\dot{r} + N_{pq}pq + N_{qr}qr] \\
&\quad + \frac{\rho}{2}L^4[N_{\dot{v}}\dot{v} + N_pup + N_rur + N_{vq}vq \\
&\quad + N_{wp}wp + N_{wr}wr] \\
&\quad + \frac{\rho}{2}L^3[N_vuv + N_{vw}vw + N_{\delta r}u^2\delta_r] \\
&\quad - \frac{\rho}{2}\int_{x_{\text{tail}}}^{x_{\text{nose}}}[C_{dy}h(x)(v + xr)^2 + C_{dz}b(x)(w - xq)^2] \\
&\quad \cdot \frac{(v + xr)}{U_{cf}(x)}xdx + (x_GW - x_BB)\cos\theta\sin\phi \\
&\quad + (y_GW - y_BB)\sin\theta + \frac{\rho}{2}L^3u^2N_{\text{prop}}.
\end{aligned}
$$

Euler Angle Rates And Global Positions, Crossflow Velocity, And Propulsion Terms

$$
\begin{aligned}
\dot{\phi} &= p + q\sin\phi\tan\theta + r\cos\phi\tan\theta \\
\dot{\theta} &= q\cos\phi - r\sin\phi \\
\dot{\psi} &= (q\sin\phi + r\cos\phi)/\cos\theta \\
\dot{X} &= u_{c0} + u\cos\psi\cos\theta \\
&\quad + v[\cos\psi\sin\theta\sin\phi - \sin\psi\cos\phi] \\
&\quad + w[\cos\psi\sin\theta\sin\phi + \sin\psi\sin\phi] \\
\dot{Y} &= v_{c0} + u\sin\psi\cos\theta \\
&\quad + v[\sin\psi\sin\theta\sin\phi + \cos\psi\cos\phi] \\
&\quad + w[\sin\psi\sin\theta\sin\phi - \cos\psi\sin\phi] \\
\dot{Z} &= w_{c0} - u\sin\theta + v\cos\theta\sin\psi \\
&\quad + w\cos\theta\sin\phi \\
U_{cf}(x) &= [(v + xr)^2 + (w - xq)^2]^{1/2} \\
X_{\text{prop}} &= C_{d0}(\eta|\eta| - 1);\ \eta = 0.012n/u; \\
C_{d0} &= 0.00385 \\
\epsilon(n) &= -1 + \text{sign}(n)/\text{sign}(u)^* \\
&\quad \cdot (\sqrt{C_t + 1} - 1)/(\sqrt{C_{t1} + 1} - 1) \\
C_t &= 0.008L^2\eta|\eta|/2.0;\ C_{t1} = 0.008L^2/2.0
\end{aligned}
$$

Table of Parameters

$W = 53.4$ kN	$B = 53.4$ kN	$L = 5.3$ m	$I_z = 13587$ Nms^2
$I_{xy} = -13.58$ Nms^2	$I_{yz} = -13.58$ Nms^2	$I_{xz} = -13.58$ Nms^2	$I_y = 13587$ Nms^2
$I_x = 2038$ Nms^2	$x_G = 0.0$	$x_B = 0.0$	$y_G = 0.0$
$y_B = 0.0$	$z_G = 6.1$ cm	$z_B = 0.0$	$g = 9.81$ m/s^2
$\rho = 1000$ kg/m^3	$m = 5454.54$ kg		
$X_{pp} = 7.0e-3$	$X_{qq} = -1.5e-2$	$X_{rr} = 4.0e-3$	$X_{pr} = 7.5e-4$
$X_{\dot{u}} = -7.6e-3$	$X_{wq} = -2.0e-1$	$X_{vp} = -3.0e-3$	$X_{vr} = 2.0e-2$
$X_{q\delta s} = 2.5e-2$	$X_{q\delta b/2} = -1.3e-3$	$X_{r\delta r} = -1e-3$	$X_{vv} = 5.3e-2$
$X_{ww} = 1.7e-1$	$X_{v\delta r} = 1.7e-3$	$X_{w\delta s} = 4.6e-2$	$X_{w\delta b/2} = 0.5e-2$
$X_{\delta s\delta s} = -1e-2$	$X_{\delta b\delta b/2} = -4e-3$	$X_{\delta r\delta r} = -1e-2$	$X_{q\delta sn} = 2.0e-3$
$X_{w\delta sn} = 3.5e-3$	$X_{\delta s\delta sn} = -1.6e-3$		
$Y_{\dot{p}} = 1.2e-4$	$Y_r = 1.2e-3$	$Y_{pq} = 4e-3$	$Y_{qr} = -6.5e-3$
$Y_{\dot{v}} = -5.5e-2$	$Y_p = 3.0e-3$	$Y_r = 3.0e-2$	$Y_{vq} = 2.4e-2$
$Y_{wp} = 2.3e-1$	$Y_{wr} = -1.9e-2$	$Y_v = -1.0e-1$	$Y_{vw} = 6.8e-2$
$Y_{\delta r} = 2.7e-2$			
$Z_{\dot{q}} = -6.8e-3$	$Z_{pp} = 1.3e-4$	$Z_{pr} = 6.7e-3$	$Z_{rr} = -7.4e-3$
$Z_{\dot{w}} = -2.4e-1$	$Z_q = -1.4e-1$	$Z_{vp} = -4.8e-2$	$Z_{vr} = 4.5e-2$
$Z_w = -3.0e-1$	$Z_{vv} = -6.8e-2$	$Z_{\delta s} = -7.3e-2$	$Z_{\delta b/2} = -1.3e-2$
$Z_{qn} = -2.9e-3$	$Z_{wn} = -5.1e-3$	$Z_{\delta sn} = -1.0e-2$	
$K_{\dot{p}} = -1.0e-3$	$K_{\dot{r}} = -3.4e-5$	$K_{pq} = -6.9e-5$	$K_{qr} = 1.7e-2$
$K_{\dot{v}} = 1.3e-4$	$K_p = -1.1e-2$	$K_r = -8.4e-4$	$K_{vq} = -5.1e-3$

(Continued) TABLE OF PARAMETERS

$K_{wp} = -1.3e-4$	$K_{wr} = 1.4e-2$	$K_v = 3.1e-3$	$K_{vw} = -1.9e-1$
$K_{\delta b/2} = 0.0$	$K_{pn} = -5.7e-4$	$K_{\text{prop}} = 0.0$	
$M_{\dot{q}} = -1.7e-2$	$M_{pp} = 5.3e-5$	$M_{pr} = 5.0e-3$	$M_{rr} = 2.9e-3$
$M_{\dot{w}} = -6.8e-2$	$M_{uq} = -6.8e-2$	$M_{vp} = 1.2e-3$	$M_{vr} = 1.7e-2$
$M_{uw} = 1.0e-1$	$M_{vv} = -2.6e-2$	$M_{\delta s} = -4.1e-2$	$M_{\delta b/2} = 3.5e-3$
$M_{qn} = -1.6e-3$	$M_{wn} = -2.9e-3$	$M_{\delta sn} = -5.2e-3$	
$N_{\dot{p}} = -3.4e-5$	$N_{\dot{r}} = -3:4e-3$	$N_{pq} = -2.1e-2$	$N_{qr} = 2.7e-3$
$N_{\dot{v}} = 1.2e-3$	$N_p = -8.4e-4$	$N_r = -1.6e-2$	$N_{vq} = -1.0e-2$
$N_{wp} = -1.7e-2$	$N_{wr} = 7.4e-3$	$N_v = -7.4e-3$	$N_{vw} = -2.7e-2$
$N_{\delta r} = -1.3e-2$	$N_{\text{prop}} = 0.0$		

REFERENCES

[1] M. A. Abkowitz, *Stability and Motion Control of Ocean Vehicles.* Cambridge, MA: M.I.T. Press, 1969.

[2] R. J. Boncal, "A study of model based maneuvering controls for autonomous underwater vehicles," M.E. Thesis, Naval Postgraduate School, Monterey, CA, Dec. 1987.

[3] R. Cristi, F. A. Papoulias, and A. J. Healey, "Adaptive sliding mode control of autonomous underwater vehicles in the dive plane," *IEEE J. Oceanic Eng.,* vol. 15, pp. 462–470, 1991.

[4] I. W. Dand and M. J. Every, "An overview of the hydrodynamics of umbilical cables and vehicles—Parts I and II," in *Proc. Subtech '83.* Society for Underwater Technology, 1983, pp. 525–562.

[5] R. A. De Carlo, S. H. Zak, and G. P. Mathews, "Variable structure control of non-linear multivariable systems: A tutorial," *Proc. IEEE,* vol. 76, pp. 212–232, Mar. 1988.

[6] G. J. Dobeck, K. W. Watkinson, and E. H. Freeman, "Navigation, guidance, and control of an autonomous 30-foot model submarine," *Rep. NCSC TR 370-82,* Naval Coastal Systems Center, Panama City, FL, June 1982.

[7] F. Dougherty and G. Woolweaver, "At sea testing of an unmanned underwater vehicle flight control system," in *Proc. AUV 90,* IEEE Catalog No. 90CH2856-3, 1990, pp. 51–59.

[8] T. I. Fossen, "Nonlinear modeling and control of underwater vehicles," Dr. Ing. Thesis, Norwegian Institute of Technology, Trondheim, 1991.

[9] T. I. Fossen and S. Sagatun, "Adaptive control of nonlinear systems: A case study of underwater robotic systems," *J. Robotic Systems,* vol. 8, pp. 393–412, 1991.

[10] D. Humphries, "Dynamics and hydrodynamics of ocean vehicles," in *IEEE Oceans '81 Conf. Proc.,* vol. 1, pp. 88–91, 1981.

[11] M. Gertler and G. R. Hagen, "Standard equations of motion for submarine simulations," *NSRDC Rep. 2510,* 1967.

[12] K. R. Goheen, E. R. Jefferys, and D. R. Broome, "Robust self designing controllers for underwater vehicles," *Trans. ASME J. Offshore Mechanics and Arctic Eng.,* vol. 109, pp. 170–178, May 1987.

[13] G. F. Gueler, "Modelling, design and analysis of an autopilot for submarine vehicles," *Int. Shipbuilding Progress,* vol. 36, pp. 51–85, 1989.

[14] D. J. Lewis, J. M. Lipscomb, and P. G. Thompson, "The simulation of remotely operated underwater vehicles," in *Proc. ROV '84,* The Marine Technology Society, San Diego, CA, pp. 245–252, 1984.

[15] E. V. Lewis, ed., *Principles of Naval Architecture—Vol III.* The Society of Naval Architects and Marine Engineers, 1988.

[16] D. Lienard, "Sliding mode control for multivariable AUV autopilots," M.E. Thesis, Naval Postgraduate School, Monterey, CA (available through NTIS), June 1990.

[17] A. G. Lindgren, D. B. Cretella, and A. F. Bessacini, "Dynamics and control of submerged vehicles," *Trans. Instrument Society of America,* vol. 6, pp. 335–346, Dec. 1967.

[18] G. L. Milliken, "Multivariable control of an underwater vehicle," M.S. Thesis, MIT, Cambridge, MA, 1984.

[19] F. A. Papoulias, "Bifurcation analysis of line of sight guidance using sliding modes," *Int. J. Bifurcation and Chaos,* vol. 1, 1991.

[20] ——, "Stability considerations of guidance and control laws for AUV's in the horizontal plane," in *Proc. 7th UUST,* pp. 140–158, 1991.

[21] R. J. Richards and D. P. Stoten, "Depth control of a submersible vehicle," *Int. Shipbuilding Progress,* vol. 28, pp. 30–39, Feb. 1981.

[22] G. T. Russel and J. Bugge, "Adaptive estimator for the automatic guidance of an unmanned submersible," *Proc. Inst. Elec. Eng.,* vol. 128, pt. D., pp. 223–226, Sept. 1981.

[23] M. J. Ruth and D. E. Humphreys, "A robust multivariable control system for low speed UUV operation," in *Proc. AUV '90,* IEEE Catalog No. 90CH2856-3, pp. 51–59, 1990.

[24] J. J. E. Slotine and J. A. Coetsee, "Adaptive sliding mode controller synthesis for nonlinear systems," *Int. J. Contr.,* vol. 42, 1986.

[25] N. S. Smith, J. W. Crane, and D. C. Summey, "SDV simulator hydrodynamic coefficients," *NCSC Rep. TM-231-78,* June 1978.

[26] J. N. Sur, "Preliminary investigations of variable structure controls for the NPS model 2 AUV," M.S. Thesis Naval Postgraduate School, Monterey, CA (available through NTIS), June 1989.

[27] V. I. Utkin, "Variable structure systems with sliding modes," *IEEE Trans. Automat. Contr.,* vol. AC-22, pp. 212–222, Apr. 1977.

[28] D. R. Yoerger and J. J. E. Slotine, "Robust trajectory control of underwater vehicles," *IEEE J. Oceanic Eng.,* vol. 10, pp. 462–470, Oct. 1985.

[29] D. R. Yoerger, J. B. Newman, and J. J. E. Slotine, "Supervisory control system for the JASON ROV," *IEEE J. Oceanic Eng.,* vol. 11, pp. 392–400, 1986.

[30] D. R. Yoerger, J. G. Cooke, and J. J. E. Slotine, "The influence of thruster dynamics on underwater vehicle behavior and their incorporation in design," *IEEE J. Oceanic Eng.,* vol. 15, pp. 167–179, 1991.

[31] D. B. Young, "Model investigation of the stability and control characteristics of the contract design for the deep submergence rescue vehicle (DSRV)," *Rep. 3030,* David Taylor Research Center, Bethesda, MD, Apr. 1969.

[32] J. Yuh, "Modeling and control of underwater vehicles," *IEEE Trans. Syst., Man, Cybern.,* vol. 20, pp. 1475–1483, 1990.

Anthony J. Healey graduated from London and Sheffield Universities with the degrees B.Sc.(Eng) and Ph.D. in mechanical engineering in 1961 and 1966 respectively.

He emigrated to the US in 1966 and has taught at The Pennsylvania State University, MIT, The University of Texas at Austin, and the Naval Postgraduate School. He was promoted to Full Professor of Mechanical Engineering in 1974 at the University of Texas at Austin, and in 1981, he joined Brown and Root, Inc. as manager of the Pipeline and Sub-Sea Technology Research Group. In 1986, he returned to academe serving two terms (until 1992) as Professor and Chairman of Mechanical Engineering at the US Naval Postgraduate School. His areas of specialty include System Dynamics and Intelligent Control, and he is presently the Director of the NPS Autonomous Underwater Vehicle Project.

Dr. Healey is a Fellow of ASME and Past Chairman of the ASME Dynamic Systems and Control Division.

David Lienard received the BA degree in math and physics from Illinois College in 1974, an MBA Degree from the University of Central Florida in 1983 while assigned as an instructor at Naval Nuclear Power School in Orlando, and a Masters in Mechanical Engineering and the Mechanical Engineer Degree from the Naval Postgraduate School, where he began his study of sliding mode control theory.

He joined the Navy in 1979 after teaching high school in Lincoln, Illinois. He is currently an Engineering Duty Officer stationed at the Supervisor of Shipbuilding Office, Newport News, Virginia.